Journal of Thermal Analysis and Calorimetry
https://doi.org/10.1007/s10973-018-7811-9

Experimental investigation and thermal modelling of box and parabolic type solar cookers for temperature mapping

F. Yettou[1] · A. Gama[1] · B. Azoui[2] · A. Malek[3] · N. L. Panwar[4]

Received: 5 April 2018 / Accepted: 7 October 2018

Abstract

This investigation examines mathematical modelling and experimental validation of two types of solar cookers: a box type with tilted intercept area equipped with one external reflector, and a parabolic cooker with a new configuration. Experiments were carried out with the cookers filled with two kilograms of water from 08:00 to 15:00 solar time. During the experiments, temperature gain in the box-type solar cooker was recorded at about 69.8 °C and in the parabolic-type solar cooker at 73.6 °C at the stagnation point. Direct normal irradiation in three distinct study areas was observed and found that it varied from 7.6 to 10 kWh m^{-2}. Cooking pot placed in parabolic cooker was varied between 130 and 132 °C. Centre and south-east regions of study areas where global irradiation varied from 8 to 8.4 kWh m^{-2} were found suitable for box-type solar cooker and cooking pot temperature were found in the range of 100 °C to 105 °C. Mathematical modelling was programmed in MATLAB. The theoretical results were consistent with experiential data for both types of solar cookers. The effectiveness of the two cooker types can be deduced from the maps. It is found the use of the cookers in Northern and Southern regions of the country was not identical. Their suitability for cooking depends on the amount of solar radiations received.

Keywords Solar radiation · Box solar cooker · Parabolic solar cooker · Thermal model · Experimental tests · Temperature maps

List of symbols

φ, λ	Geographical latitude, longitude (rad)
z	Elevation above sea level (m)
γ_s, γ_s^{cor}	Solar altitude and corrected solar altitude angle (rad)
θ_z, θ_{az}	Solar zenith and azimuth angle (rad)
I_0 (= 1367), G_0	Solar constant and extra-terrestrial solar irradiance (W m^{-2})
IN	Direct normal irradiance (W m^{-2})
IB_h, ID_h, IG_h	Beam, diffuse and global irradiance on horizontal surface
IB_h	Beam radiation reflected to the absorber of BSC (W m^{-2})
IS, IR	Solar flux available on cookers (W m^{-2})
T_{rd}, F_d	Diffuse transmission, diffuse sky irradiance distribution function (–)
T_L, T_L (AM2)	Linke turbidity and corrected Linke factor (–)
m_A, δ_R	Relative optical air mass and Rayleigh optical thickness of the atmosphere (–)

✉ F. Yettou
yettou.t@gmail.com

1 Unité de Recherche Appliquée en Energies Renouvelables, URAER, Centre de Développement des Energies Renouvelables, CDER, 47133 Ghardaïa, Algeria

2 LEB Laboratory, Electrotechnics Department, Faculty of Technology, University of Batna2, Rue Chahid Med El Hadi Boukhlouf, 05000 Batna, Algeria

3 Centre de Développement des Energies Renouvelables, CDER, 16340 Algiers, Algeria

4 Department of Renewable Energy Engineering, Maharana Pratap University of Agriculture and Technology, Udaipur, Rajasthan 313001, India

Published online: 13 October 2018

θ_{Bg}, θ_{Rp}	Angles of reflected sun rays (rad)
ψ	Rim angle (rad)
α, β, θ	Angles related to booster mirror (rad)
L_1, L, L', H, H', h, W_h, W_i, W, W'	Various lengths shown in Fig. 5 (m)
D, d, d_p, F, f	Various lengths shown in Fig. 6 (m)
T_a, T_s	Ambient, sky temperature (°C)
T_g, T_i, T_p, T_v, T_f	Glass cover, air inside, absorber plate, cooking vessel, cooking fluid temperature related to BSC (°C)
T_{ref}, T_{pot}, T_{wat}	Parabolic reflector, outside wall cooking pot, cooking fluid related to PSC (°C)
Q_c, Q_r	Convective and radiation heat flux (W)
Q, U	Thermal losses (W)
h_c, h_r	Convective and radiation heat coefficient (W m^{-2} K^{-1})
mc_p	Heat capacity (J K^{-1})
A_g, A_{eff}, A_{vb}, A_p, A_v, A_{vf}, A_{sw}, A_{ref}, A_{spot}, A_{pot}, A_{pf}	Area (m^2)
α_g, α_p, α_v, α_{ref}, α_{pot}	Absorptivity (–)
τ_g, ρ_B	Transmissivity and reflectivity (–)
ε, F_{Bg}	Factors (–)
W_s	Wind speed (m s^{-1})

Introduction

In the present context, energy is considered a key issue in economic development of the nation. Annually, energy consumption increases by an average of 1% in developed countries and 5% in developing countries [1, 2]. Consumption of fossil fuels is dramatically growing along with the increasing world population, improvements in the quality of life, and industrialization of developing nations. This excessive fossil fuel consumption leads to an increase in the rate of diminishing fossil fuel reserves, causing serious world environmental problems like pollution, global warming and climate change. Thus, renewable energy sources have attracted great interest at the international level during recent years in order to meet the world's growing energy demands and to reduce greenhouse gas emissions [3]. Among the renewable energy sources, solar energy is at the head of these technologies, and it is expected to play a very significant role in the developing and developed countries in addressing energy security and environmental concerns.

Solar cooking is one of the most significant solar energy applications. Solar energy is a promising option capable of being one of the leading energy sources for cooking [4]. Presently, energy required for cooking represents about 36% of the global primary energy consumption [5–7]. The solar cooker has great potential in the domestic sector. Extensive research has been conducted in recent history, especially during the last 4 years [8] by many scientists, researchers and academicians regarding design development of and experimentation with solar cookers. The literature reveals a variety of different types of cookers, such as the box type and the concentrating type. Furthermore, many improved designs for solar cookers are continuously being proposed, requiring continual update of solar cooker classifications, the most recent classification being proposed by Yettou et al. [1].

Thermal modelling and parametric study are another aspect of solar cooker design, which is important in predicting temperatures and the thermal behaviour of solar cookers. Much research has recently been reported globally concerning conventional box-type solar cookers [9–13]. Nevertheless, few studies have been done on mathematical modelling of the box-type solar cooker with a tilted intercept area [14], especially with external reflectors (booster mirrors) added to the cooker, and limited literature is available on mathematical modelling of parabolic solar cooker. In the present, the study focuses on the development of a mathematical model of a box-type solar cooker with tilted intercept area (BSCTIA) equipped with one external reflector and a parabolic solar cooker (PSC) with a new configuration design in order to determine the thermal behaviour in both cookers. The parabolic solar cooker (PSC) was configured in such a way that focal point becomes a focal area. It resolves the issues of food burning at a concentration point.

Experimental

Development of solar radiation map

To estimate solar irradiation incident on the cookers surface, clear sky model of the European Solar Radiation Atlas (ESRA) for Heliosat method suggested by Rigollier et al. [15] was used. The solar irradiation model r.sun is an efficient tool for estimating solar irradiation for clear sky and overcast atmospheric conditions [16]. Standard solar radiation equations as proposed by Kreith and

Kreider [17] and Duffie and Bechman [18] were used to develop the solar radiation map. Different angles used to calculate the solar energy available for box-type and parabolic-type solar cookers are illustrated in Fig. 1.

Thermal modelling

The various heat transfer modes in the two considered cookers are illustrated in Fig. 2. To develop a mathematical model of these cookers, possible heat transfer routes are identified; an energy balance equation for heat transfer routes was determined. The following assumptions are made to simplify the model:

1. The PSC cooking pot support's (grid) is constructed in such a manner so that it allows to takeover reflected rays from parabolic reflector to cooking pot easily. Thus, its effect on the heat transfer process is negligible.
2. There is proper thermal contact between cooking vessel and absorber surface of the cooker.
3. Reflective heat transfer between cooker sidewalls and cooking vessel is negligible.
4. The heat exchange due to air inside the lid covered vessel is not taken into account.

As BSC as concerns, the heat transfer model is based on using energy balance over five different components of the cooker: The energy balance equations are as follows:

Energy balance at glass cover:

$$(mc_p)_g \frac{dT_g}{dt} = \tau_g \alpha_g A_g IS + Q_{c,i\to g} + Q_{r,v\to g} + Q_{r,p\to g} - Q_{c,g\to a} - Q_{r,g\to s} \quad (1)$$

Energy balance of air inside the cooker:

$$(mc_p)_i \frac{dT_i}{dt} = Q_{c,p\to i} + Q_{c,v\to i} - Q_{c,i\to g} \quad (2)$$

Energy balance at absorber plate:

$$(mc_p)_p \frac{dT_p}{dt} = \tau_g \alpha_p A_{eff} IS - Q_{r,p\to g} - Q_{c,p\to i} - Q_{p\to a} - Q_{sw\to a} - Q_{p\to v} \quad (3)$$

Energy balance at vessel:

$$(mc_p)_v \frac{dT_v}{dt} = \tau_g \alpha_v n A_{vb} IS + Q_{p\to v} - Q_{c,v\to f} - Q_{r,v\to g} - Q_{c,v\to i} \quad (4)$$

Energy balance inside vessel fluid:

$$(mc_p)_f \frac{dT_f}{dt} = Q_{c,v\to f} \quad (5)$$

where

$$Q_{c,i\to g} = h_{c,i-g} A_g (T_i - T_g) \quad (6)$$

$$Q_{c,g\to a} = h_{c,g-a} A_g (T_g - T_a) \quad (7)$$

$$Q_{c,p\to i} = h_{c,p-i} (A_p - nA_{vb})(T_p - T_i) \quad (8)$$

$$Q_{c,v\to i} = h_{c,v-i} n A_v (T_v - T_i) \quad (9)$$

$$Q_{c,v\to f} = h_{c,v\to f} n A_{vf} (T_v - T_f) \quad (10)$$

$$Q_{r,v\to g} = h_{r,v-g} n A_{vb} (T_v - T_g) \quad (11)$$

$$Q_{r,p\to g} = h_{r,p-g} (A_p - nA_{vb})(T_p - T_g) \quad (12)$$

$$Q_{r,g\to s} = h_{r,g-s} A_g (T_g - T_s) \quad (13)$$

$$Q_{p\to a} = U_{pa} A_p (T_p - T_a) \quad (14)$$

$$Q_{sw\to a} = U_{sw} A_{sw} (T_p - T_a) \quad (15)$$

$$Q_{p\to v} = U_{vb} n A_{vb} (T_p - T_v) \quad (16)$$

Replacing the heat transfer flux, we obtain the following equations:

– For glass cover:

$$(mc_p)_g \frac{dT_g}{dt} = \tau_g \alpha_g A_g IS + h_{c,i-g} A_g (T_i - T_g) + h_{r,v-g} n A_{vb} (T_v - T_g) + h_{r,p-g} (A_g - nA_{vb})(T_p - T_g) - h_{c,g-a} A_g (T_g - T_a) - h_{r,g-s} A_g (T_g - T_s) \quad (17)$$

– For air inside the cooker:

$$(mc_p)_i \frac{dT_i}{dt} = h_{c,p-i} (A_p - nA_{vb})(T_p - T_i) + h_{c,v-i} n A_v (T_v - T_i) - h_{c,i-g} A_g (T_i - T_g) \quad (18)$$

– For absorber plate:

$$(mc_p)_p \frac{dT_p}{dt} = \tau_g \alpha_p A_{eff} IS - h_{r,p-g} (A_p - nA_{vb})(T_p - T_g) - h_{c,p-i} (A_p - nA_{vb})(T_p - T_i) - (U_{pa} A_p + U_{sw} A_{sw})(T_p - T_a) - U_{vb} n A_{vb} (T_p - T_v) \quad (19)$$

– For vessel:

$$(mc_p)_v \frac{dT_v}{dt} = \tau_g \alpha_v n A_{vb} IS + U_{vb} n A_{vb} (T_p - T_v) - h_{c,v-f} n A_{vf} (T_v - T_f) - h_{r,v-g} n A_{vb} (T_v - T_g) - h_{c,v-i} n A_v (T_v - T_i) \quad (20)$$

– For vessel fluid:

$$(mc_p)_f \frac{dT_f}{dt} = h_{c,v\to f} n A_{vf} (T_v - T_f) \quad (21)$$

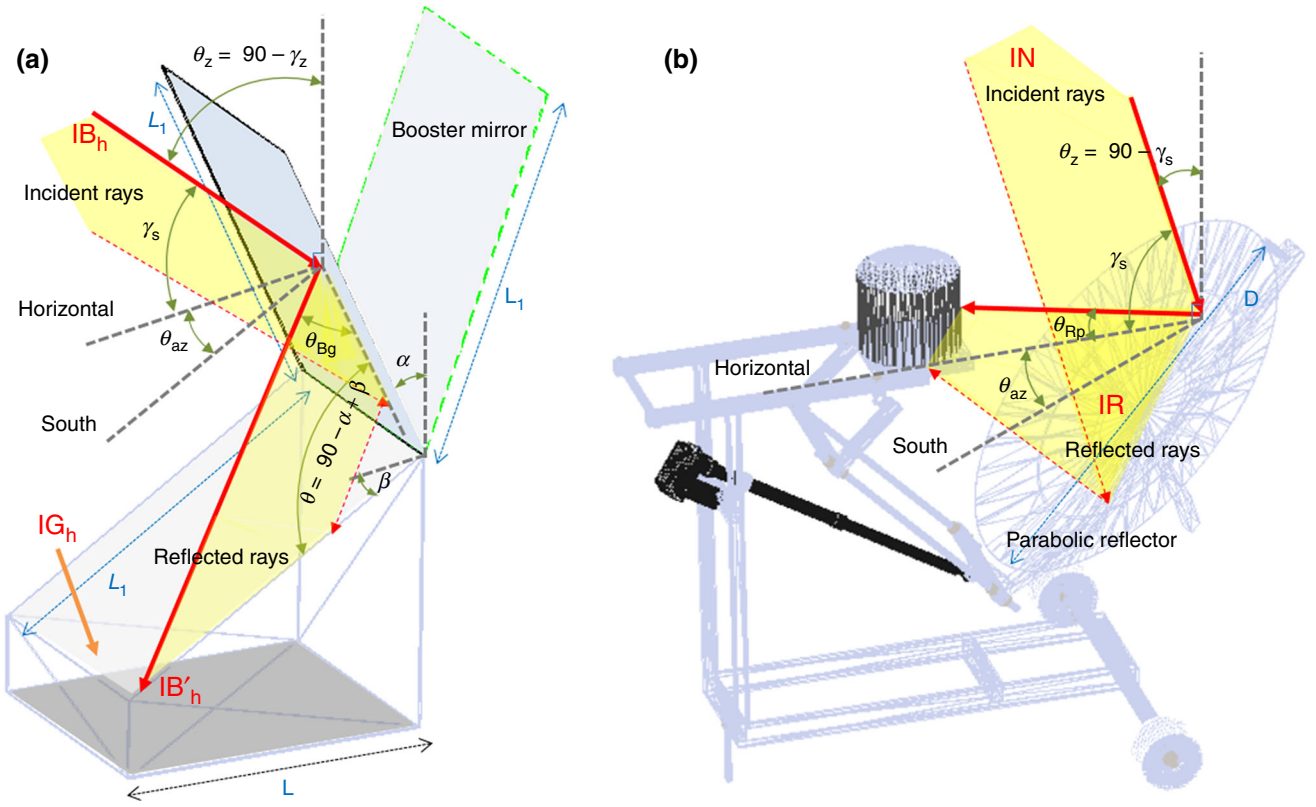

Fig. 1 Illustration of the different angles used to calculate the net solar energy available on the cooker receivers: **a** box solar cooker; **b** parabolic solar cooker

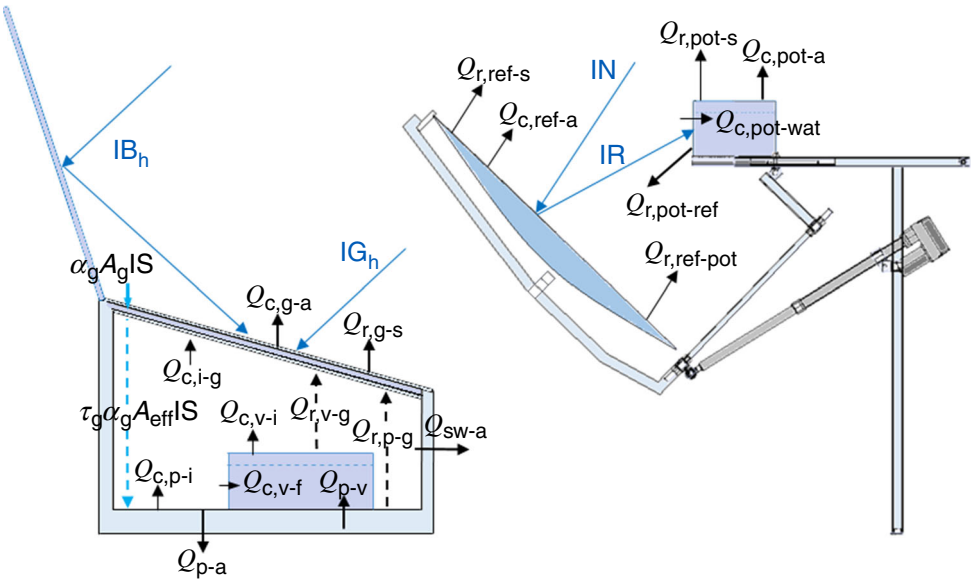

Fig. 2 Various mode of heat transfer in the box and parabolic solar cookers

Equations (17 to 21) form a coupled system of nonlinear differential equations for variables T_g, T_i, T_p, T_v and T_f of the BSC.

Concerning PSC, the heat transfer model is based on using energy balance over three components of the cooker. The energy balance equations are presented as follows:

Energy balance at parabolic reflector:

$$(mc_p)_{ref}\frac{dT_{ref}}{dt} = \alpha_{ref}A_{ref}IN + Q_{r,ref\to pot} - Q_{c,ref\to a} - Q_{r,ref\to s} \quad (22)$$

Energy balance at vessel:

$$(mc_p)_{pot}\frac{dT_{pot}}{dt} = \alpha_{pot}A_{spot}IR - Q_{c,pot\to wat} - Q_{c,pot\to a} - Q_{r,ref\to pot} - Q_{r,pot\to s} \quad (23)$$

Energy balance inside vessel fluid:

$$(mc_p)_{wat}\frac{dT_{wat}}{dt} = Q_{c,pot\to wat} \quad (24)$$

where

$$Q_{c,ref\to a} = h_{c,ref-a}A_{ref}(T_{ref} - T_a) \quad (25)$$

$$Q_{c,pot\to a} = h_{c,pot-a}A_{pot}(T_{pot} - T_a) \quad (26)$$

$$Q_{c,pot\to wat} = h_{c,pot-wat}A_{pf}(T_{pot} - T_{wat}) \quad (27)$$

$$Q_{r,ref\to pot} = h_{r,pot-ref}A_{ref}(T_{pot} - T_{ref}) \quad (28)$$

$$Q_{r,pot\to s} = h_{r,pot-s}A_{pot}(T_{pot} - T_s) \quad (29)$$

$$Q_{r,ref\to s} = h_{r,ref-s}A_{ref}(T_{ref} - T_s) \quad (30)$$

By replacing the heat transfer flux, we obtain the following equations:

– For reflector:

$$(mc_p)_{ref}\frac{dT_{ref}}{dt} = \alpha_{ref}A_{ref}IN + h_{r,pot-ref}A_{ref}(T_{pot} - T_{ref}) - h_{c,ref-a}A_{ref}(T_{ref} - T_a) - h_{r,ref-s}A_{ref}(T_{ref} - T_s) \quad (31)$$

– For vessel:

$$(mc_p)_{pot}\frac{dT_{pot}}{dt} = C_R\alpha_{pot}A_{spot}IN - h_{c,pot-wat}A_{pf}(T_{pot} - T_{wat}) - h_{c,pot-a}A_{pot}(T_{pot} - T_a) - h_{r,pot-ref}A_{ref}(T_{pot} - T_{ref}) - h_{r,pot-s}A_{pot}(T_{pot} - T_s) \quad (32)$$

– For vessel fluid:

$$(mc_p)_{wat}\frac{dT_{wat}}{dt} = h_{c,pot-wat}A_{pf}(T_{pot} - T_{wat}) \quad (33)$$

Equations (31–33) also form a coupled system of nonlinear differential equations for variables T_{ref}, T_{pot} and T_{wat} of the PSC.

Net solar energy available on the glass cover of the box cooker and on the cooking pot of the parabolic reflector can be calculated using standard solar radiation equations as proposed by Kreith and Kreider [17] and Duffie and Bechman [18].

To predict cooker temperature, model was developed in MATLAB and desired input is taken from Table 1. Flow chart of MATLAB programme to predict solar radiation and cooker temperatures is presented in Fig. 3.

Description of the realized solar cookers

Box-type solar cooker

The realized BSCTIA was made of a wooden box, and the hot box was made from a mirror sheet. The dimensions of the hot box are 500 mm × 400 mm × 445 mm × 125 mm, and the overall dimensions are 550 mm × 450 mm × 495 mm × 175 mm above the ground. The absorber is made of an aluminium sheet painted matt black which absorbs the solar radiation and transfers the heat to the cooking pots. A single glass cover with a wooden frame is placed over it. The space between the outer box and inner tray, including the bottom of the tray, is packed with insulating material (in this case, glass wool) in order to reduce heat losses from the cooker. The aluminium cooking pot (18 cm in diameter and 10 cm in height) is cylindrical in shape, filled with water, painted and equipped with a black cover, and placed into the solar box cooker. One external reflector (550 mm × 450 mm) with an adjustable arm was provided; it serves as a booster mirror, enhancing the temperature of the hot box. The solar radiation falls onto the glass lid and passes through it to strike the absorber plate. The inside air, in contact with the absorber, warms up and transmits its heat to the cooking pot which then transfers the heat to cook the food.

As designed and developed, the box-type solar cooker with tilted intercept area (BSCTIA) has several advantages when compared to conventional box cookers with only horizontal collecting surfaces (Fig. 4); to minimize the width of the shadow strip on the absorber by increasing the effective width of the sun rays intercepted by the absorber plate ($W_i > W_h$), which can be mathematically demonstrated as follows:

From Fig. 5 and using simple trigonometric relationships, we have:

$$W_h = L' \cdot \sin(\gamma_s) \quad (34)$$

$$W_i = L_1 \cdot \cos(90 - \gamma_s - \beta) \quad (35)$$

According to the standard of box-type solar cooker [19], the size of the booster mirror must be the same as the base of the cooker (Fig. 4a). For our case (Fig. 4b), since the lid mirror should cover the entire surface of the cooker, the booster mirror must be of the same length of the glazed surface, thus:

$$L_1 = \frac{L}{\cos(\beta)} \approx \frac{L'}{\cos(\beta)} \quad (36)$$

By replacing the expression of L_1 in Eq. (35), we obtain the formula (37) for calculating the width of intercepted sun rays W_i which is always superior than W_h (Eq. 34):

Table 1 Input parameters for computation

Parameters	Value	Parameters	Value
$(mc_p)_g$	2241	A_{vf}	0.005
$(mc_p)_i$	52.36	A_{sw}	0.196
$(mc_p)_p$	2485	A_{ref}	0.63
$(mc_p)_v$	7605	A_{pot}	0.0628
$(mc_p)_f$	4185 or 8370	A_{pf}	0.005
$(mc_p)_{ref}$	3279	α_g	0.06
$(mc_p)_{pot}$	7605	α_p	0.9
$(mc_p)_{wat}$	4185 or 8370	α_v	0.9
A_g	0.329	α_{ref}	0.06
A_p	0.196	α_{pot}	0.9
A_v	0.0628	τ_g	0.88
A_{vb}	0.0314		

$$W_i = L' \cdot \frac{\sin(\gamma_s + \beta)}{\cos(\beta)} \tag{37}$$

Parabolic-type solar cooker

As shown in Fig. 5, the realized parabolic solar cooker (PSC) refers to a point focusing concentrator that consists of a parabolic reflector supported by a stand, and a cooking pot placed at the focal point of the cooker. The reflector is a paraboloid-shaped type with 0.9 m as its aperture diameter. This solar cooker has a steel structure and uses small mirror facets as a reflector. The reflective area of the solar cooker is 0.63 m^2, the focal length of the cooker is 0.5 m and the focal area of the cooker is 0.10 m^2. The concentration ratio for the dish calculates at about 10 in which 240 small mirror segments are joined to form the collector. The reflectivity of the mirror facets is 0.88. The aluminium cooking pot (20 cm in diameter and 10 cm in height) was filled with water and equipped with a black cover placed at the focus point of the cooker.

The whole PSC system is designed in such a manner as to have a new structural support compared to the ordinary PSC. The parabolic reflector and the black pot are separated from each other. This configuration permits the resolving of one of the inconveniences of conventional PSCs, namely overflow of content when the cooker is adjusted to follow the sun.

The second advantage of this configuration is that the PSC is designed with a modified focal point which becomes a focal area. In the conventional PSC, due to a high solar flux for a very small area food burns at the concentration point. It is also very difficult to maintain the position of the concentrated spot instantaneously at the focal point during cooking time, which then leads to having frequently readjust the cooker (every 5 min). This situation is tiring for users, especially when the conventional PSCs use a manual mode for sun tracking. In addition, the prolonged time is needed for cooking food because of the inefficiency of those cookers. From an optical point view, the losses are higher in such a design and thus a lower concentration factor. In order to reduce the needed corrections of the ray path and improve the concentration factor, the focal point area must increase. This problem was solved by moving the cooking pot a distance f from the focal point to produce a focal rounder area with a d_p that is then diameter associated with a movable cooking vessel support (see illustrated scheme in Fig. 5).

The mathematical formulas for calculating the new focal distance f from the parabolic vertex are as follows:

$$\tan\psi = \frac{d_p/2}{f} = \frac{D/2}{F-d} \tag{38}$$

The parametric equation of the parabola is:

$$d = \frac{1}{4F} \cdot \frac{D^2}{2} \tag{39}$$

By inserting Eq. (39) into Eq. (38) and solving the equation, the new focal point distance from the parabolic vertex is known by calculating the value of f as follows:

$$f = \frac{(F-d) \cdot d_p}{D} \tag{40}$$

Instrumentation and measurements

The performance evaluation of developed cookers was executed at the Applied Research Unit on Renewable Energies affiliated with the Center of Renewables Energies Development, located in Ghardaïa, south Algeria (32.39°N, 3.78°E, 463 m above sea level) under clear sky conditions during several seasons of the years 2016 and 2017. Figure 6 provides a photographic view of the experimental box and parabolic solar cookers in Ghardaïa (Algeria).

The ambient temperature in °C was measured with a Campbell CS215 temperature instrument. The water temperatures were measured with K-type thermocouples because of their height accuracy and rapid response. The wind speed was measured with an NRG 40H Anemometer. The global solar radiation was recorded with a Kipp & Zonen CMP21 pyranometer while direct normal irradiances were measured with a Kipp &Zonen CHP1 pyrheliometer. A data-logger, AGILENT 34972A was used to take the readings. The recorded data were stored in a computer for storage on disk and viewing on screen. Figure 7 shows the data acquisition system used to test the realized cookers.

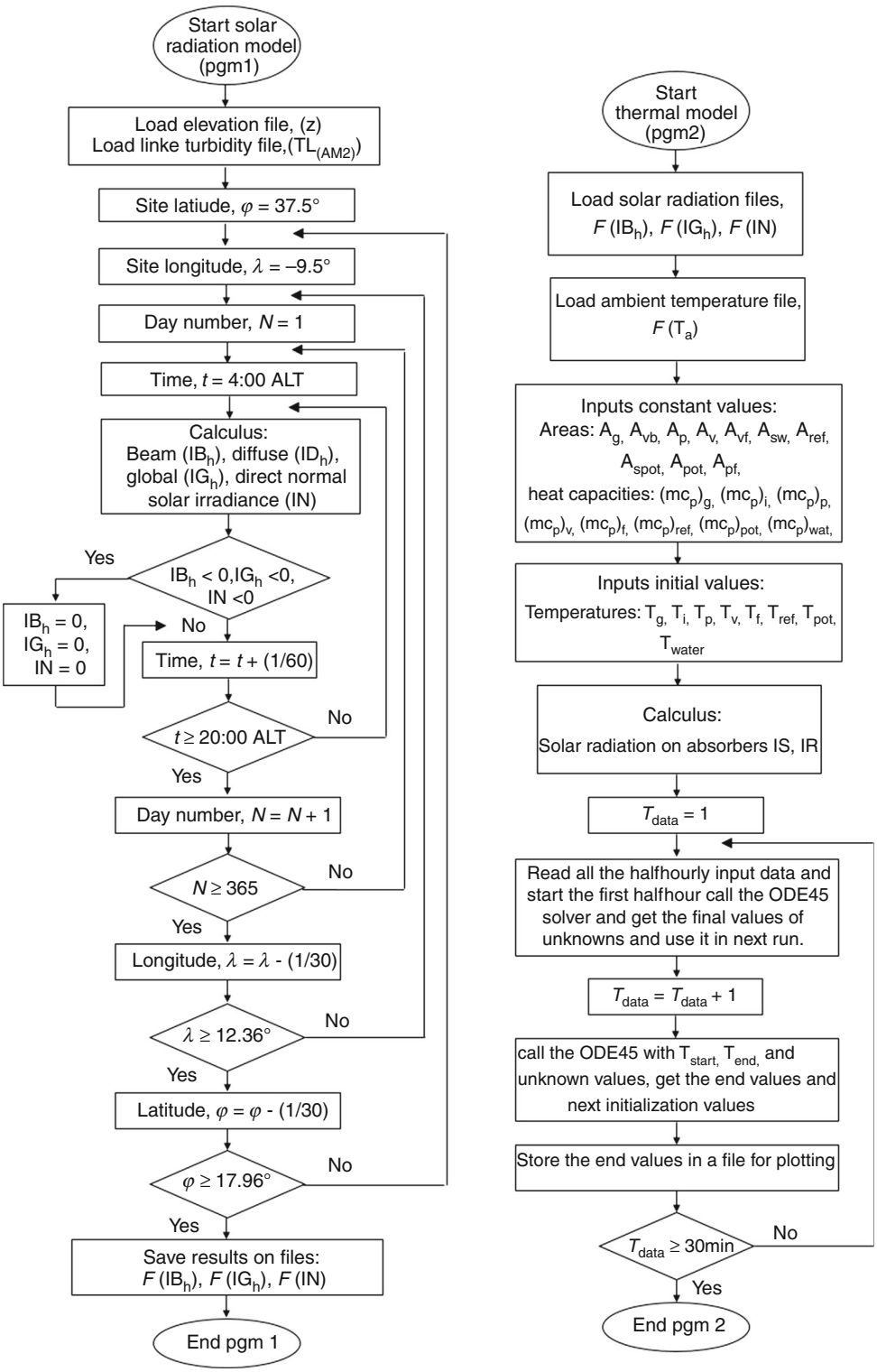

Fig. 3 Chart of the solar irradiation and thermal model programme

Manual solar tracking was done, which meant, the position of the cookers in relation to the sun has to be adjusted every 30 min so that the angle between the incident sun rays and the lateral walls of the box cookers was always equal to 0. In addition, the angular position of the reflector α had to be changed in relation to the sun elevation so that it faced the sun. The angle θ (as shown in Fig. 1a) was used to adjust the booster mirror from the

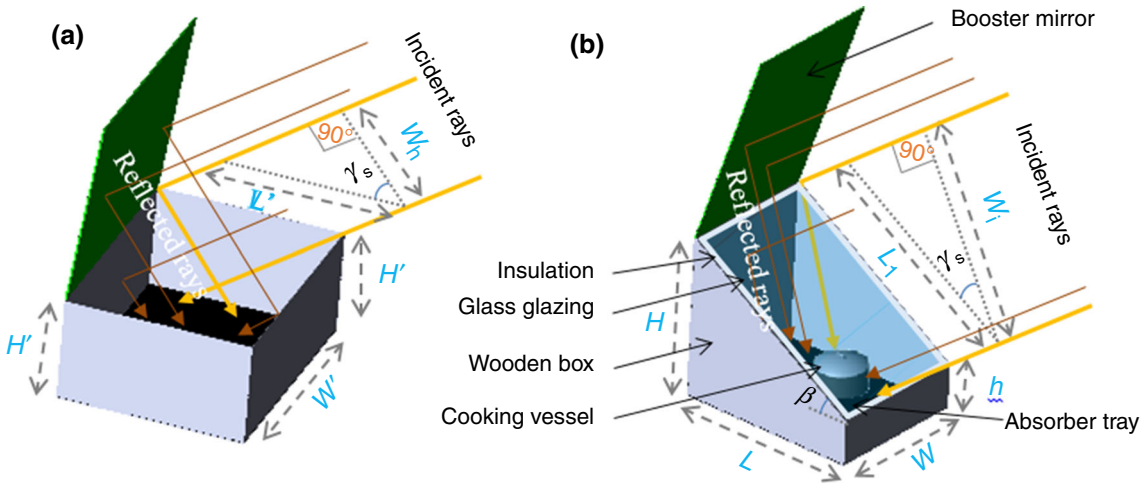

Fig. 4 A schematic diagram of optical sun rays incidents on the absorber of the box solar cooker with tilted intercept area compared to the conventional box solar cooker with horizontal collecting surface

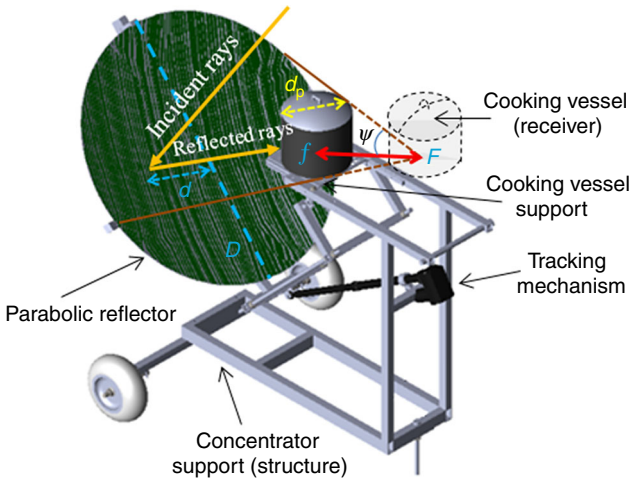

Fig. 5 A 3D View of the new configuration design for parabolic solar cooker

cooker lid (tilted glazed surface taken as reference). In the test on the parabolic cooker, the incident sun rays always had to be perpendicular to the aperture area of the concentrator.

In order to draw temperature maps of the box and parabolic cookers, a digital terrain model was used which was based on raster data from the digital terrain elevation model (DTEM) and vector data from the digital chart of the world (DCW) [20]. Linke turbidity factor (T_L) was assessed, using monthly T_L (AM2) values, which was retrieved for each month from the Solar Radiation Database for Environment (SoDa) project website [21] for 200 points (locations) evenly spread over the study region.

Results and discussion

Thermal performance

Experimental measurements

In 2016 and 2017, temperature profiles were measured and recorded to assess the thermal performance of BSC and PSC under different climatic conditions. The profile was collected in the city of Ghardaïa (south Algeria) using an aluminium cooking pot filled with 2 kg of water. This is the optimum load used in cooking food for a single family. Two representative thermal water heating profiles will subsequently be illustrated for thermal model validation purpose.

Figure 8 presents the experimental and the predicted water temperatures for the BSC with the available solar flux. Figure 9 presents the experimental and predicted water temperatures for the PSC with a variation in the solar radiation. Data for Figs. 8 and 9 were collected in January of 2017. January and December are considered winter months in Algeria's climatic conditions. Low solar radiation and fewer sunshine hours are available during this time of year and the daily average ambient temperatures can be as low as until 5 °C in Ghardaïa.

On the test day of 30 January 2017, the ambient temperature varied from 10 to 16.1 °C. The solar flux available on the tilted glass cover of BSC varied from 389 to 1486 W m^{-2}. The maximum solar flux, estimated at 13:00, was 1497 W m^{-2}, while the solar radiation incident on the PSC's reflector varied from 676 to 965 W m^{-2} with a maximum of 968 W m^{-2} recorded at 13:00. Figures 8 and 9 show that, despite the low initial vessel fluid temperature for both types of solar cookers, as the time increases, the

Fig. 6 A photographic view of the realized box solar cooker with tilted intercept area and the new structural design of parabolic solar cooker

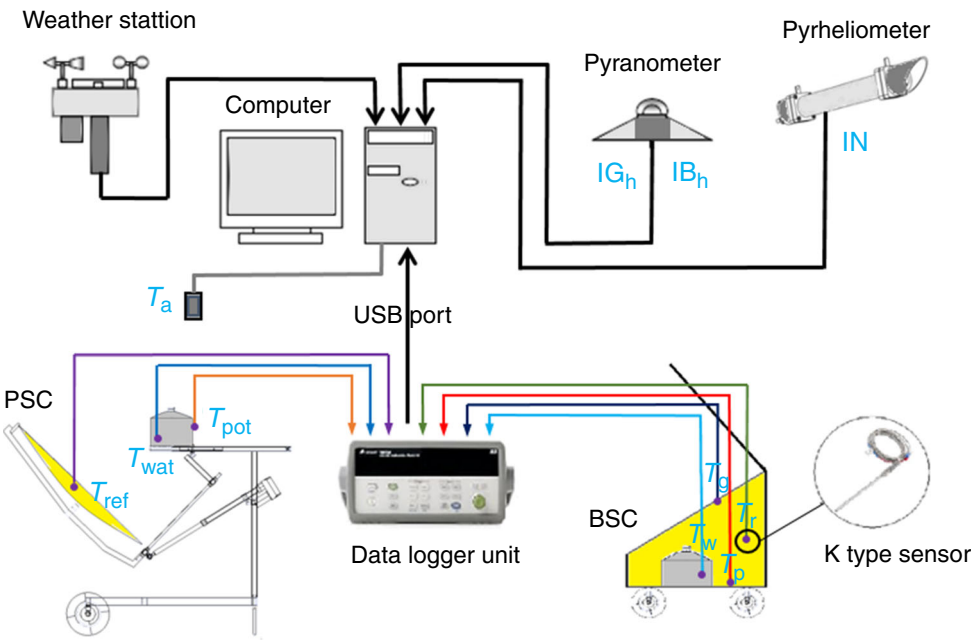

Fig. 7 Schematic of the data acquisition system used for experimentation of the realized solar cookers

fluid temperature increases to the peak and reaches to stagnant level as the water temperature approaches the optimum level, i.e., near the boiling point.

For BSC, the experimental fluid temperature varied from 15.1 to 84.9 °C, while predicted values varied from 13.8 to 67.7 °C at 12:30. The experimental net temperature gain by the water was about 69.8 °C, and 54 °C with predicted values, which is lower than the experimental gain. For PSC, initial vessel fluid temperature was recorded at about 22.1 °C and it reached 95.8 °C at 11:00. A 73.6 °C experimental temperature gain was measured. The predicted vessel fluid temperature was approximately 4 °C to 9 °C higher or lower than that of an experimental value. The net temperature gain with predicted values was about 73.8 °C. Such a temperature gain shows that both cookers are able to prepare food for a family, with different cooking time, even in the winter month when solar radiation is low.

From the results of Figs. 8 and 9, it can be seen; in the case of winter month, when solar radiation is low, that the experimental temperature achieved for 2 kg water for box-type and parabolic-type solar cooker was 38.9° C and 76.5°, respectively. Therefore, temperature was higher in the case a of parabolic-type solar cooker due to high quantity of concentrated solar radiation received by the PSC cooking pot (IR = 8470 W m^{-2}) transferred to the

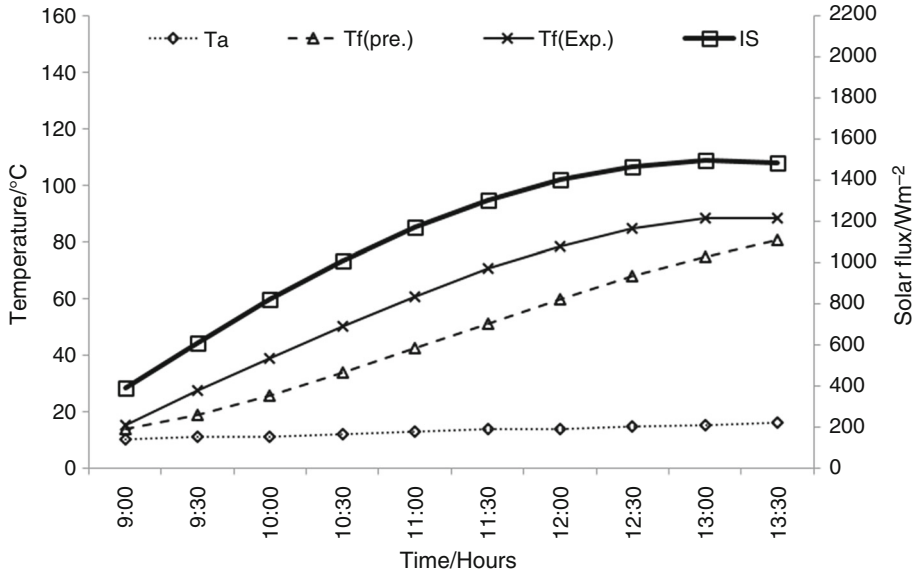

Fig. 8 Variation of experimental, predicted water temperature and available solar flux on BSC with local time for the experiment conducted on winter month's day (30 January 2017)

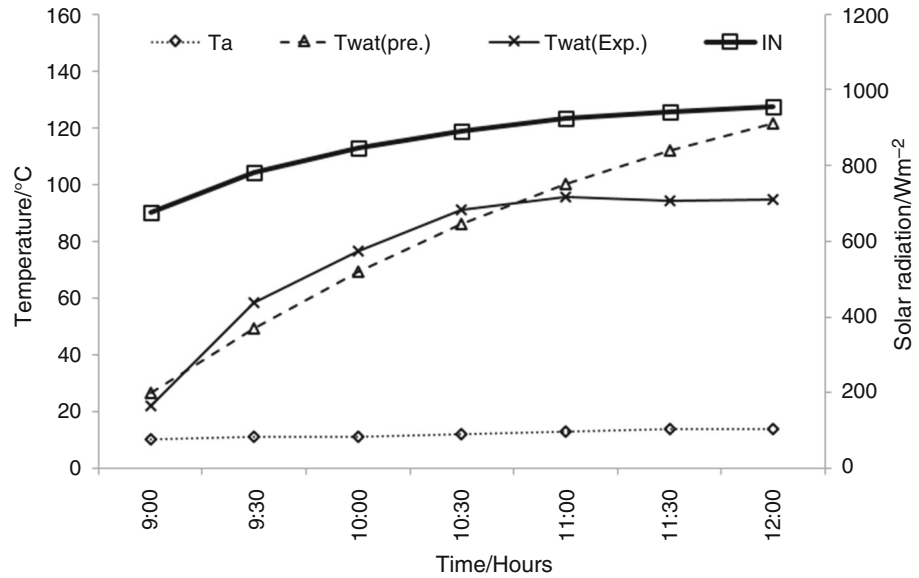

Fig. 9 Variation of experimental, predicted water temperature and direct normal solar radiation on PSC with local time for the experiment conducted on winter month's day (30 January 2017)

fluid, compared to the low solar flux intensity received by the BSC cooking pot ($IB_h^{'}$ = 818 W m^{-2}).

Figures 10 and 11 reveal the variation of water temperature in box and PSC, respectively, during summer season's days (May and July) of the year 2016. The site under consideration is characterized by an arid climate during the period from the May to September months, and the daily average ambient temperatures can reach 41 °C in July month. Therefore, the July month is considered as an extreme summer month in Algeria's climatic conditions.

The ambient temperature varied from 24.6 to 35 °C, while solar flux varied from 1107 to 1922 W m^{-2} for BSC. The direct normal solar radiation varied from 663 to 784 W m^{-2} on PSC's receiver for the test day, which can be seen in Figs. 10 and 11, respectively. Initial vessel fluid temperature during summer test for box and parabolic measured as 19.8 °C and 27.6 °C, which then reached 88.6 °C and 85.6 °C at 11:30 and 10:00, respectively. Hence, approximately 68.8 °C temperature gain was recorded with experimental values for BSC and 58 °C for PSC at the stagnation point. As far as the predicted temperature is concerned, the initial value of the vessel fluid temperatures was approximately equal to the ambient temperature and reached 88.7 °C at 11:30 h (BSC) and 77.3 °C at 10:00 h (PSC). The predicted gain of these cookers during the summer months was found to be 65.4 °C (in 2.5 h) and 41.9 °C (in 1 h), respectively, Thus, considerable temperature gain by vessel cooking fluid is observed during this month for both cooker types.

In this case also, the fluid temperature increases with time and reaches approximately stagnant level as the temperature reaches near boiling point with faster than in winter months for both cookers. It can be observed from the results, that in summer month after 1 h of sun exposure experimental temperature reaches 85.6 °C and 59.9 °C for parabolic-type and box-type solar cooker, respectively. Therefore, as explained above in this case also, cooking fluid temperature of parabolic-type cooker is considerably higher than that of the box-type cooker.

Figures 8, 9, 10 and 11 reveal that the time taken to attain the stagnant level for box-type and parabolic-type solar cooker in the winter month test's day is approximately 3 h 30 min and 2 h, respectively, and in case of the summer test day, it is about 2 h 30 min and 1 h, respectively. Therefore, it is found that the time to attain fluid temperature stagnant level for box solar cooker is higher than the parabolic solar cooker for the two seasons. Hence, as expected, the cooking of food for family can be faster in PSC than that of the BSC.

Figures 12 and 13 depict the variation of receiver temperatures and solar insolation with respect to time in both types of solar cookers, respectively, for 2 kg of water during April 2017 spring month. The month of April had clear skies as well as good sunshine and ambient temperature increases moderately as compared to winter season.

From Figs. 12 and 13, it can be observed that the ambient temperature varied from 23.4 to 31.3 °C in April test day. As far as the solar radiation is concerned, it increases with respect to time and achieved peak value at 12:15 and then again starts decreasing. The maximum beam, global and direct normal was about 1010 W m^{-2}, 761 W m^{-2} and 793 W m^{-2}, respectively. The results show that the temperature of absorber plate of BSC increases with the time until it attains the maximum value 121.9 °C at 12:30 h, (IS = 1771 W m^{-2}, T_a = 29.7 °C), whereas the corresponding predicted plate temperature was about 121.9 °C. The net experimental plate temperature was about 100.5 °C and 86.6 °C with predicted values. This temperature profile shows that on clear sunny day, the BSC is capable of cook boiling-type food. For PSC, experimental and predicted cooking pot temperature was found about 85.2 °C and 87.1 °C, respectively, reached at 11:00. There was a rise in cooking pot temperature by 51 °C experimentally and 51.9 °C with predicted values.

The low values in PSC pot temperatures compared to BSC because the thermocouple sensor is not directly exposed to solar radiation, because the height intensity of concentrated solar flux will immediately destroy the sensor; therefore, the type K thermocouple is stuck on the opposite side of cooking pot. Due to this reason, this type of solar cooker is adequately used for frying and grilling purposes.

Statistical analysis

The root mean square error (RSME), standard error (SE) and coefficient of correlation (r) were calculated to assess the feasibility and accuracy of the developed mathematical model. These three statistical parameters were used to compare simulated and experimentally obtained values (Table 2).

Coefficient of correlation values during the month of January for the box and parabolic solar cookers (Figs. 8, 9 respectively) was 0.99 and 0.98, respectively, indicating that the developed model is capable of predicting water temperatures that closely match experimental values. The standard error (SE) of box-type and parabolic cookers was

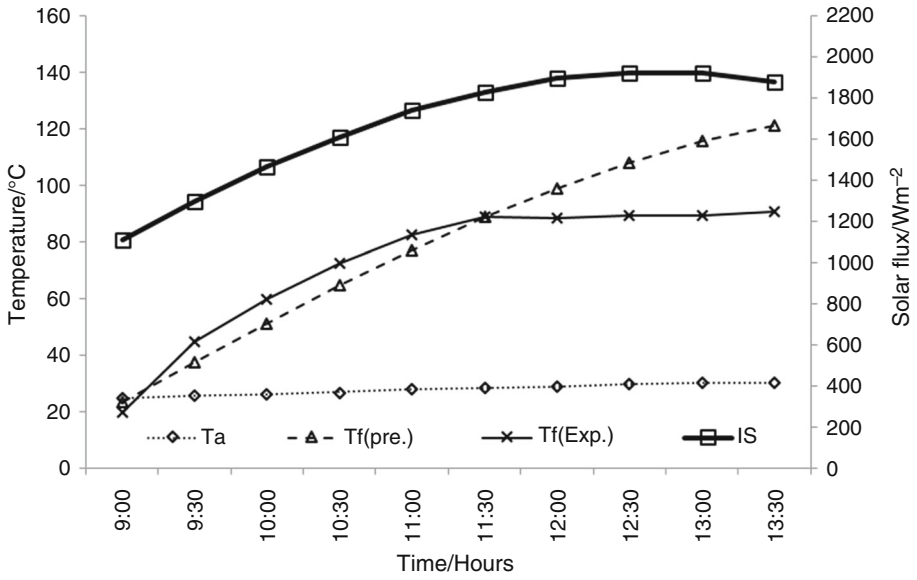

Fig. 10 Variation of experimental, predicted water temperature and available solar flux on BSC with local time for the experiment conducted on summer month's day (29 May 2016)

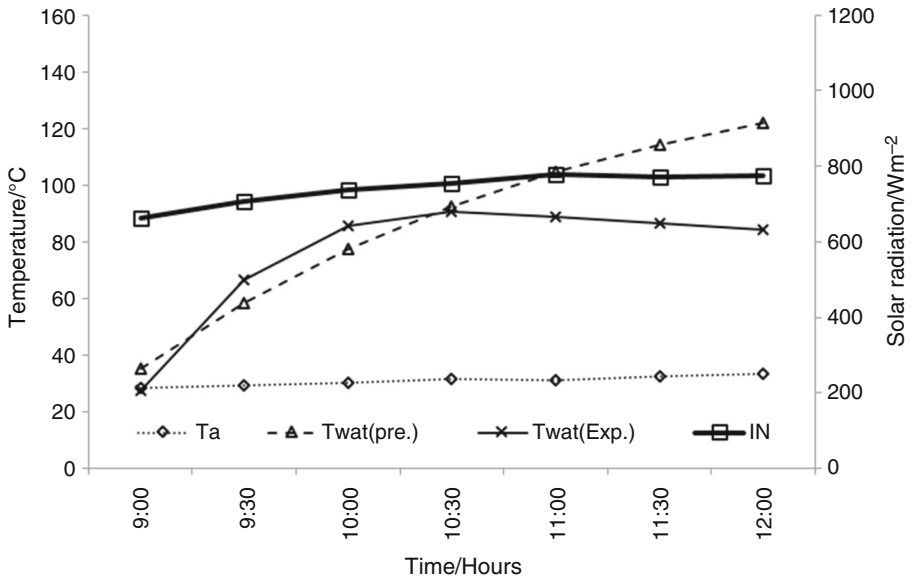

Fig. 11 Variation of experimental, predicted water temperature and direct normal solar radiation on PSC with local time for the experiment conducted on summer month's day (18 July 2016)

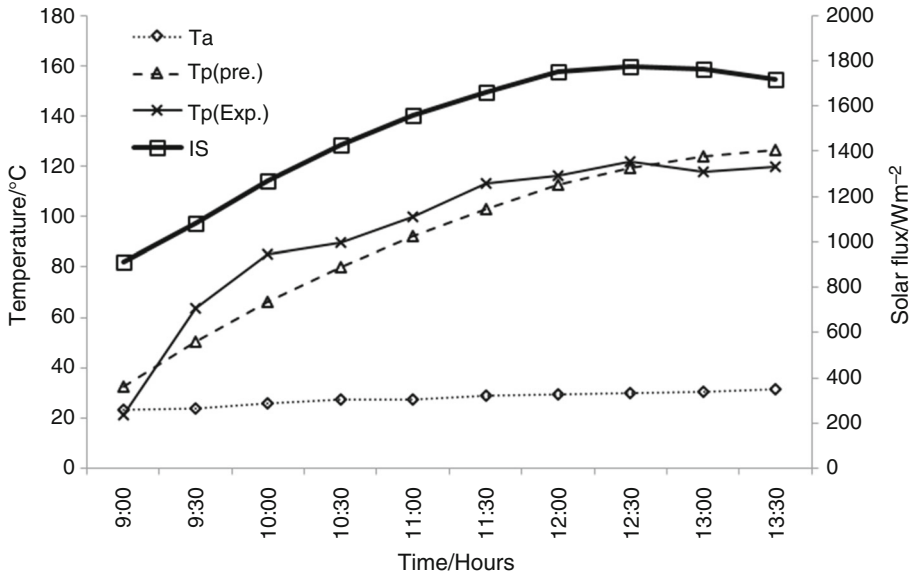

Fig. 12 Variation of experimental, predicted absorber plate temperature and available solar flux on BSC with local time. Experiment was conducted on 26 April 2017.

found to be 5.40 and 2.85, respectively, whereas root mean square error (RSME) was 5.77 and 3.18, respectively, indicating close agreement between experimental and theoretical results.

For summer months with higher solar radiation and ambient temperature (Figs. 10, 11), an average coefficient of correlation 0.99 was obtained for each solar cooker. The SE in the predicted water temperatures varied between 2.55 and 4.70, while the RSME ranged between 2.79 and 5.75 for the box and parabolic cookers, respectively. Thus, the model is capable of generating highly accurate prediction of a wide variety of environmental conditions, i.e., solar radiation and external temperature. For both cookers, we also obtained a satisfactory correlation coefficient value of (0.97) for other parameters such as receiver's temperatures in other climatic conditions (spring season) with variable load (2 kg).

Results mapping

Comparative study on two different types of solar cookers, parabolic type and box type, has been carried out based on the thermal model. In order to generate receiver's water temperature maps, the study areas cover all most of the country's area; 62 points, including 48 cities with different geographic coordinates (Lat, Lon, Alt) original of Google Earth Service was selected.

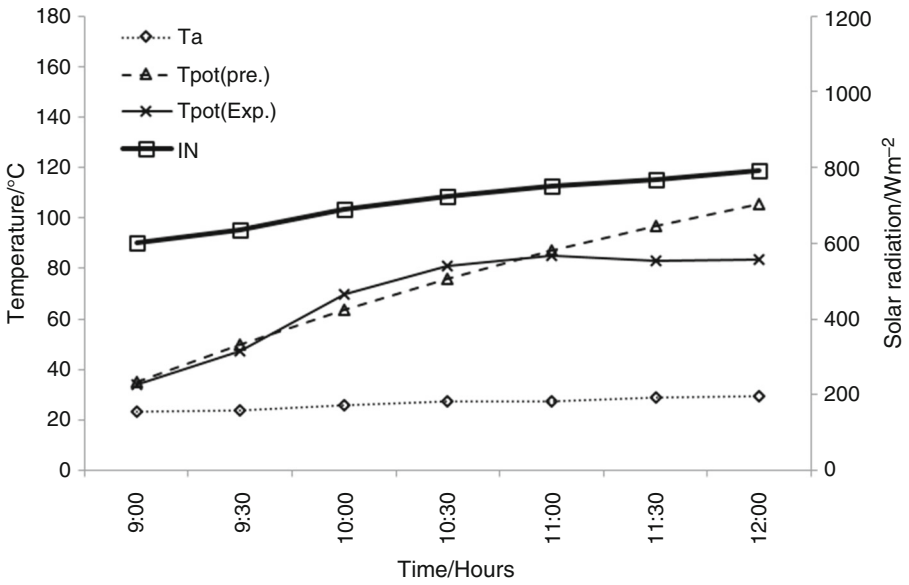

Fig. 13 Variation of experimental, predicted outside wall cooking pot receiver temperature and direct normal solar radiation on PSC with local time. Experiment was conducted on 26 April 2017.

Box and parabolic cooking pot water temperatures mapping

Water temperature in the cooking pots was attained for the summer months under a clear sky in Algeria (Figs. 14, 15). The water temperature for winter months under clear conditions is also presented (Figs. 16, 17). According to the iso-temperature distribution maps, it is clear that the solar cookers can be used in all Algerian territory in clear sky summer days (Figs. 14, 15).

For a parabolic solar cooker, there is a great potential of direct normal irradiation received by the Algerian territory during this period of year. Therefore, there are 3 distinct areas based on cooking pot temperature: (1) the best regions with a typical daily direct normal irradiation value between 9 and 10 kWh m^{-2} are situated in the south central and south-east areas of the country, with cooking pot water temperatures exceeding 135 °C; (2) direct normal irradiation values are between 8.6 and 10 kWh m^{-2} generally located at the Sahara centre and the north-west regions, with cooking pot water temperatures between 130 and 135 °C; and (3) the daily direct normal irradiation values are between 7.6 and 8.6 kWh m^{-2}, representing the centre and east littoral, east-high plains regions and the extreme south-west of the country, with water temperatures less than 130 °C.

For the box cooker, we can identify three distinct parts also: the first and best regions with cooking pot water temperatures exceeding 105 °C are situated at the centre and south-east regions with values of received daily global irradiation more than 8.2 kWh m^{-2}. The second part with global irradiation values between 8 and 8.4 kWh m^{-2} is situated in central belt regions with water temperatures between 100 and 105 °C. The third region with temperatures less than 100 °C is situated in east-high plains regions and littoral cities receiving a quantity of typical daily global irradiation less than 8 kWh m^{-2}.

For the winter season, the use duration of the cookers is reduced accordingly moving south to north (Figs. 16, 17) and, depending on the amount of received solar radiation. For a parabolic solar cooker, the recorded cooking pot water temperatures are between 85 and 108 °C for sites

Table 2 Statistical analysis of predicted temperature parameters

Cooker type	Predicted parameters	Season	Statistical parameters		
			Standard error (SE)	Root square mean error (RSME)	Correlation coefficient (r)
BSC	T_f	Winter	5.40	5.77	0.989
PSC	T_{wat}	Winter	2.848	3.184	0.976
BSC	T_f	Summer	2.552	2.795	0.982
PSC	T_{wat}	Summer	4.697	5.753	0.990
BSC	T_p	Spring	3.849	4.115	0.964
PSC	T_{pot}	Spring	1.659	1.855	0.985

with latitude greater than 36°N and between 85 and 119 °C. For site's latitude $32° < \varphi < 36°$N, the estimated water temperatures are above 108 °C in the south of the country ($\varphi < 32°$N). For the box cooker, the recorded cooking pot water temperatures are between 62 and 73 °C for sites with latitude greater than 36°N. These values were between 63 and 77 °C for site's within latitude $32° < \varphi < 36°$N. The estimated water temperatures are above 78 °C for the rest of the country.

Efficiency maps of the realized cookers

At the water temperature for BSC and PSC site in Algeria based on Figs. 14–17, we can deduce that the solar cookers mapping efficiency.

Summary of BSC pot water and PSC pot water temperature for the Algeria main sites in winter, spring and summer clear days is shown in Figs. 18 and 19. After 2 h of sun exposition, all site water temperatures exceeding 82 °C are favourable for solar cooking. This is illustrated with dashed lines in Figs. 18 and 19 for BSC and PSC, respectively. The final effect of box map is shown in Fig. 20. According to this map (Fig. 20), BSC effectiveness can be classified in three zones:

Zone I: which include the Sahara centre and deep south. These receive, a very high annual global radiation exceeding 2500 kWh m^{-2} $year^{-1}$ or 7 kWh m^{-2} day^{-1}, distributed almost uniformly throughout the year and characterized by high ambient temperatures. This type of Saharan climatic conditions allows an effective use of the cooker for the entire season in a year for the site with latitude less than 28°N.

Zone II: represents the north and north-west regions of the Sahara which are characterized by high annual global radiation, rendering use of the box cooker possible for much of the year with exception of winter. Thus, the cooker is useful for three seasons (spring, summer and autumn) since autumn has the same climatic characteristics as spring in Algeria.

Zone III: is comprised of the eastern-high plains and coastal regions (east and central), which characterized by an annual global radiation of about 2000 kWh m^{-2} $year^{-1}$, or 5 kWh m^{-2} day^{-1}. The high plains sites are characterized by low temperature values but slightly higher than coastal sites. The cooker is usable only during the summer and is ineffective in the winter.

For example, we cite the use of BSC at Tamanrasset or the city of Adrar (in south Sahara), where the cooker can be used throughout year. The duration of use of the cooker is diminished as one move further north. In the city of Ghardaïa (in north Sahara), for example, the cooker can be used during summer, spring and autumn (generally about 9 months). Controversy, in the city of Batna (eastern-high plains) or the capital city of Algiers (coastal region) the cooker is only effective during the summer.

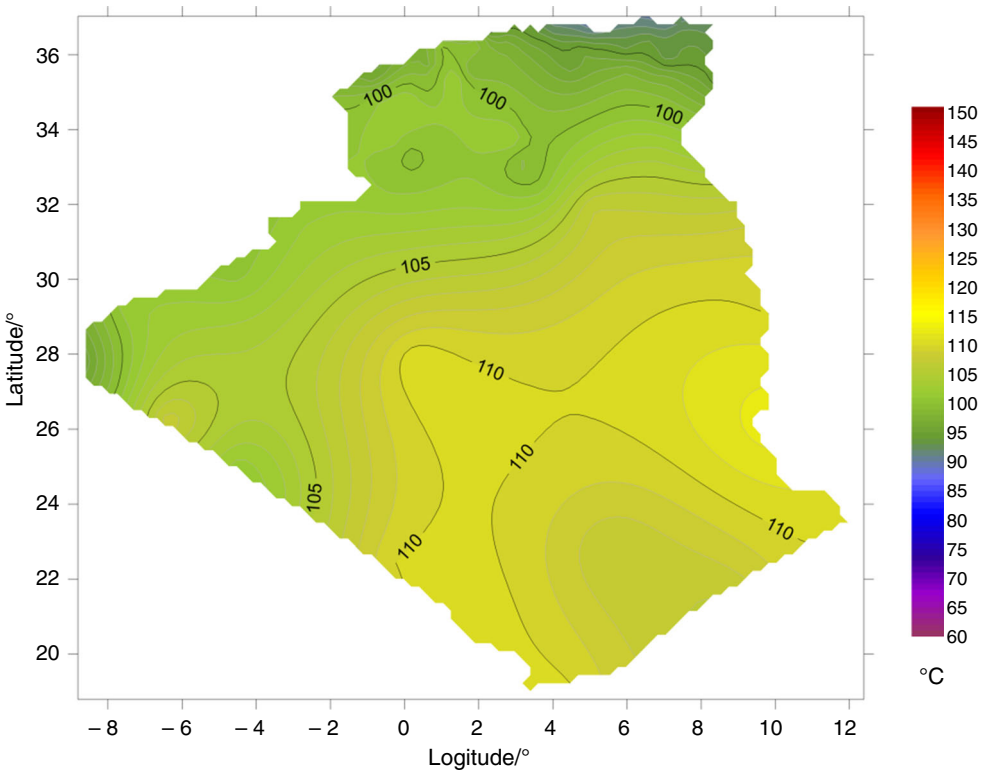

Fig. 14 Water temperature maps of BSC's cooking pot for typical clear sky summer day in Algeria

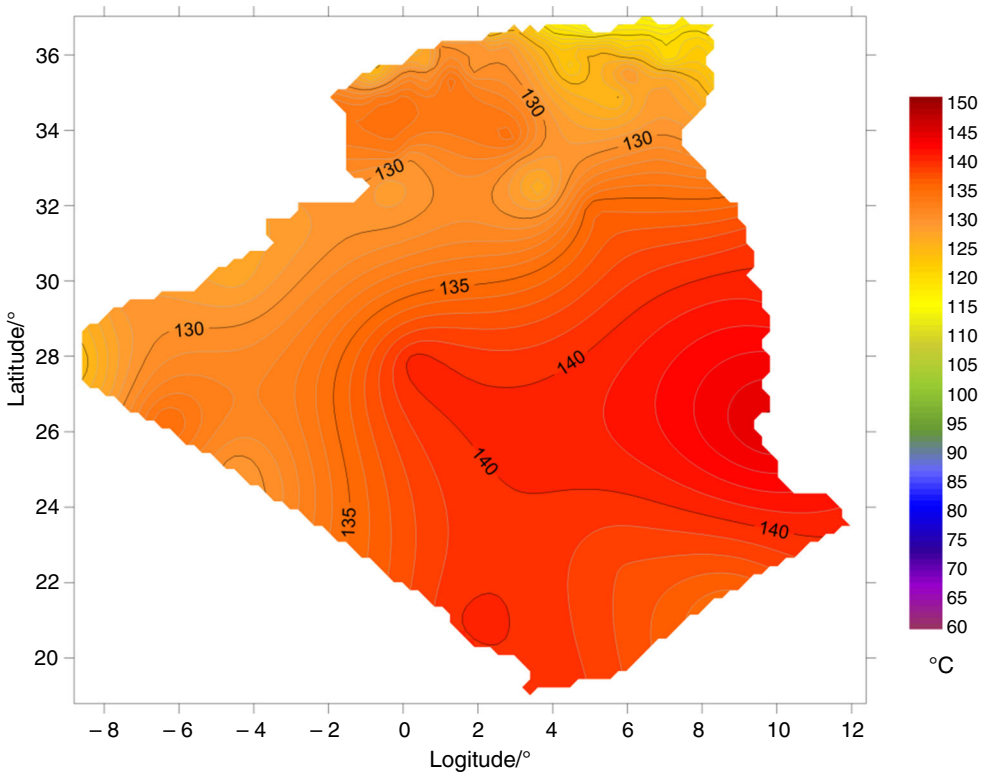

Fig. 15 Water temperature maps of PSC's receiver for typical clear sky summer day in Algeria

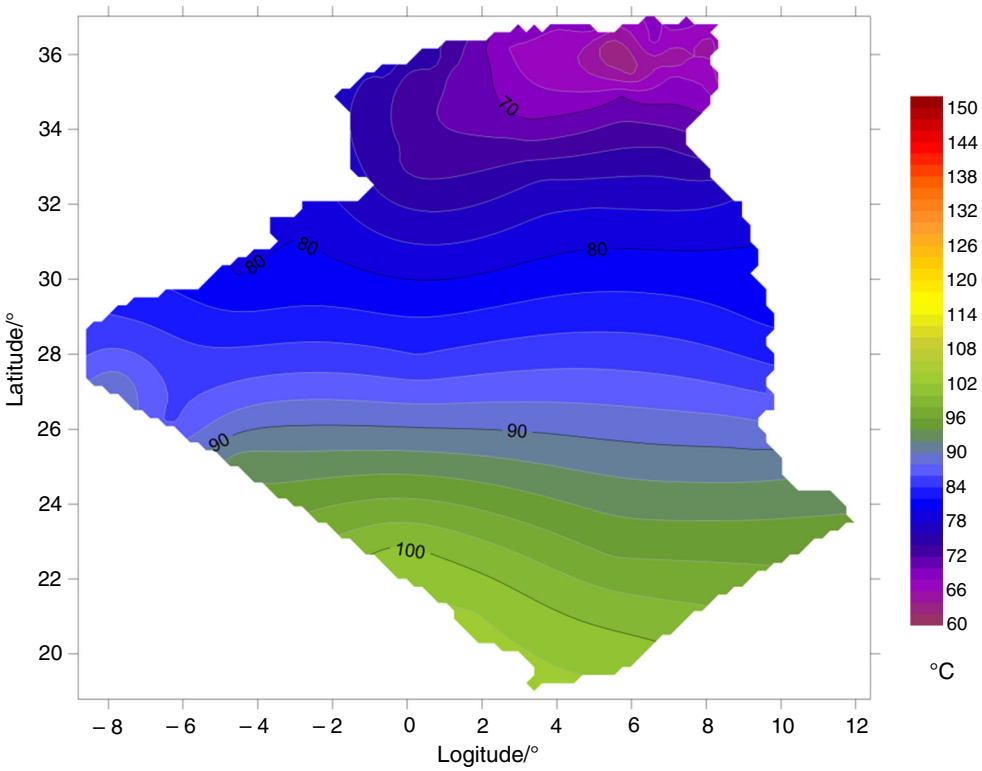

Fig. 16 Water temperature maps of BSC's cooking pot for typical clear sky winter day in Algeria

According to the results shown in Fig. 19, the PSC is exploitable throughout the entire Algerian territory during all seasons of the year, and this is the primary advantage of our realized PSC when compared to the BSC. The map demonstrating PSC effectiveness is not shown here because it is identical to that the one of BSC (Fig. 20) except that all sites are coloured red.

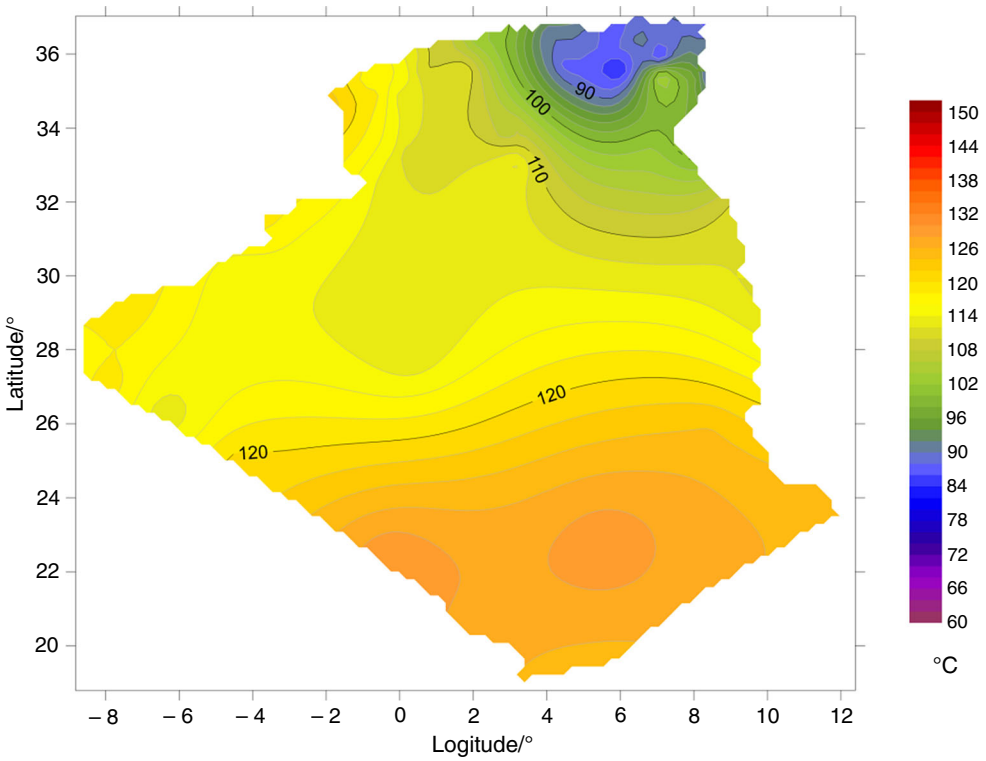

Fig. 17 Water temperature maps of PSC's receiver for typical clear sky winter day in Algeria

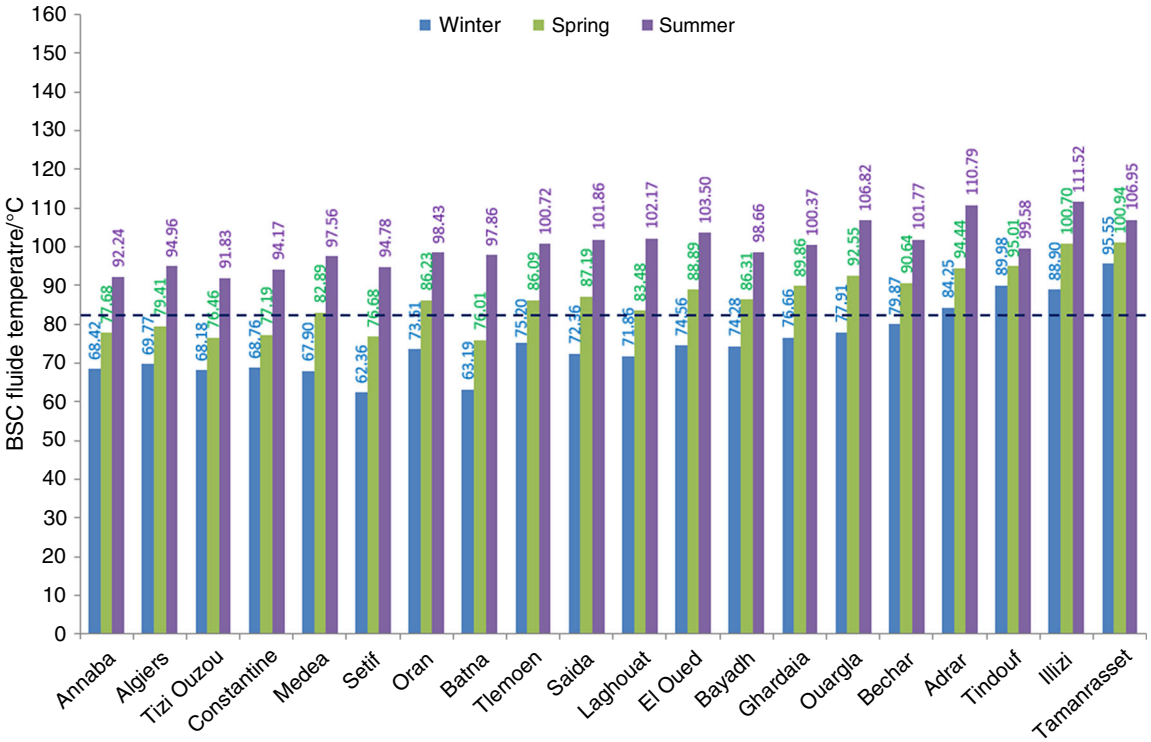

Fig. 18 Representation of water temperatures reached by the cooking pot of box solar cooker for some Algerian sites in clear days at winter, spring and summer seasons

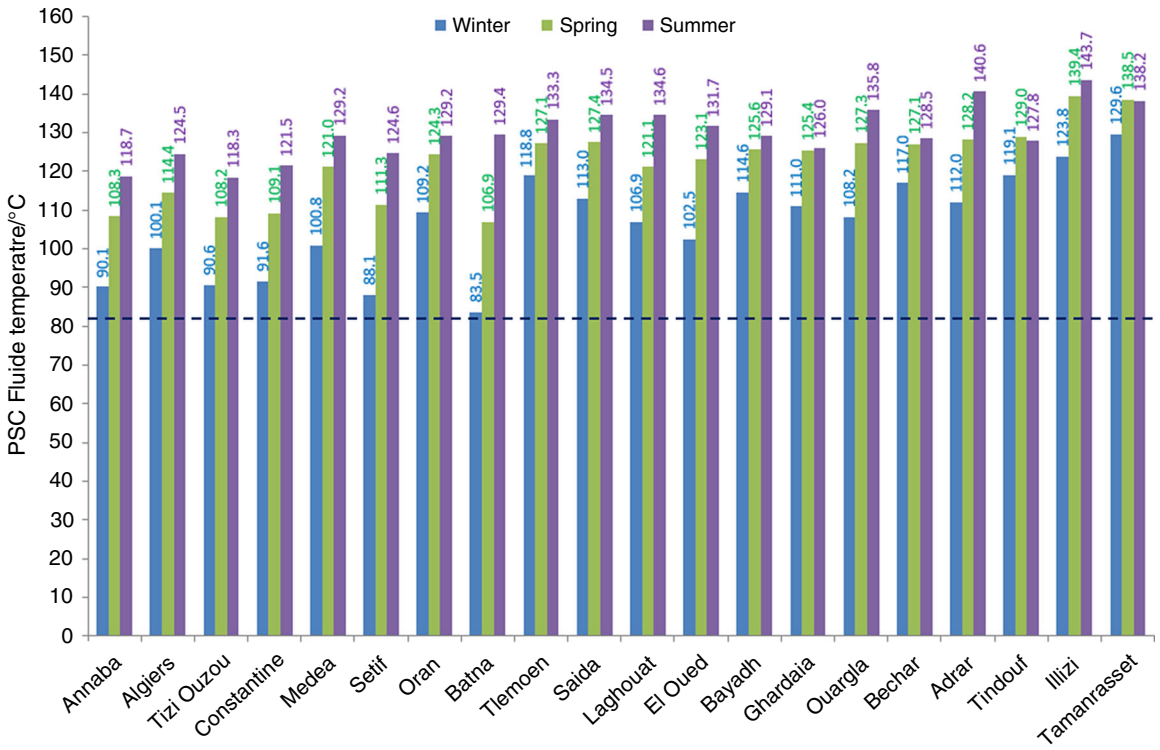

Fig. 19 Representation of water temperatures reached by the cooking pot of parabolic solar cooker for some Algerian sites in clear days at winter, spring and summer seasons

Fig. 20 Effectiveness map of BSC throughout the Algerian territory during the year

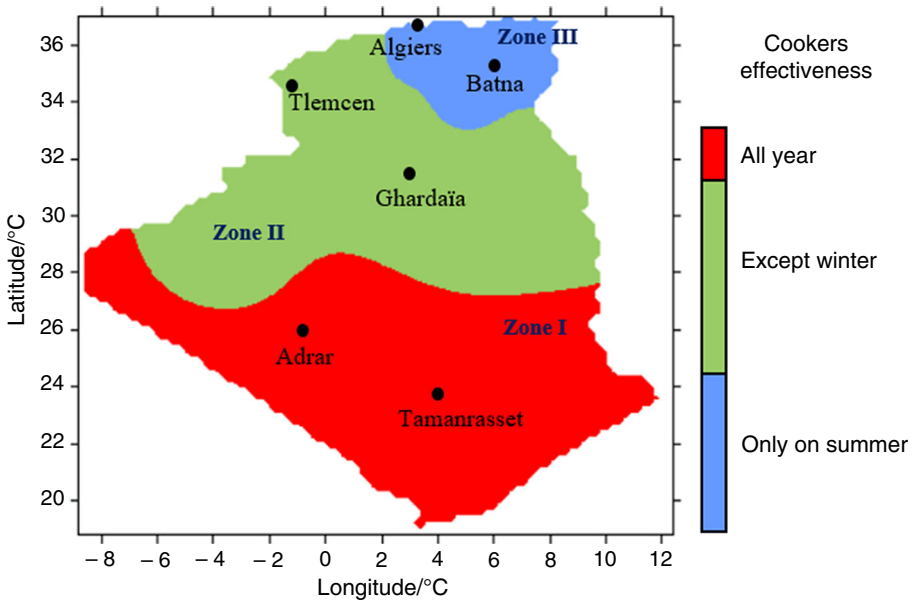

Conclusions

As the global demand for cooking energy is expected to increase greatly in coming years, solar cooking devices can play a major role in reducing or replacing energy consumption of fossil resources. In this investigation, the thermal model of a box-type solar cooker with tilted intercept area, equipped with one external reflector and a parabolic solar cooker with a new configuration, was developed based on the energy balance equations for the

temperature elements of the cookers as solved by computer numerical calculations. The developed parabolic solar cooker having the concentration ratio about 10 and configure in such a way that focal point became a focal area. This modification helps in reducing sun tracking time. The temperature of different components of the solar cookers was measured during several months, and the experimental values were compared to that predicted by the thermal model. Further coefficient of correlation was found to be 0.96 for all tests which indicated good accuracy of the mathematical model in predicting the values of predicted parameters. Another application of the thermal model is the evaluation of solar cooking potential of the solar cookers in local climatic conditions in Algeria, based on a solar radiation model and ambient temperatures. The temperature maps produced are able to predict the cookers' effectiveness during different seasons under clear skies. For BSC, the results reveal that the study region can be divided into three parts depending on the amount of received solar radiation. The PSC is exploitable throughout all Algeria territory during all seasons of the year. This indicates the high potential of solar energy for cooking food using these devices, in developing countries, as an alternative to fossil fuels.

For rentability reasons and cost-effectiveness, the aperture area of the PSC collector must be adapted to sites locations according to the available solar radiation. This will be our objectives in the next work, using a modified theoretical model, that can avoid building many physical devices, thereby saving money and time.

Acknowledgements Authors are very thankful to Renewables Energies Development Center (CDER, Algeria) and Applied Research Unit on Renewable Energies (URAER, Ghardaïa) for supporting and financing the solar cooking projects.

References

1. Yettou F, Azoui B, Malek A, Gama A, Panwar NL. Solar cooker realizations in actual use: an overview. Renew Sustain Energy Rev. 2014;37:288–306.
2. Boudghene Stambouli A, Koinuma H. A primary study on a long-term vision and strategy for the realisation and the development of the Sahara Solar Breeder project in Algeria. Renew Sustain Energy Rev. 2012;16:591–8.
3. Bellos E, Tzivanidis C. A review of concentrating solar thermal collectors with and without nanofluids. J Therm Anal Calorim. 2018. https://doi.org/10.1007/s10973-018-7183-1.
4. Panwar NL. Thermal modeling, energy and exergy analysis of animal feed solar cooker. J Renew Sustain Energy. 2013;5:043105.
5. Bansal M, Saini RP, Khatod DK. Optimal sizing of a solar–biogas-based cooking system for a cluster of villages. Int J Sustain Energy. 2014;33:1017–32.
6. Ayub I, Munir A, Amjad W, Ghafoor A, Nasir MS. Energy-and exergy-based thermal analyses of a solar bakery unit. J Thermal Anal Calorim. 2018;133(2):1001–13.
7. Ghafurian MM, Niazmand H, Ebrahimnia-Bajestan E, Nik HE. Localized solar heating via graphene oxide nanofluid for direct steam generation. J Therm Anal Calorim. 2018. https://doi.org/10.1007/s10973-018-7496-0.
8. Herez A, Ramadan M, Khaled M. Review on solar cooker systems: economic and environmental study for different Lebanese scenarios. Renew Sustain Energy Rev. 2018;81:421–32.
9. El-sebaii AA. Thermal performance of a box-type solar cooker with outer-inner reflectors. Energy. 1997;22(10):969–78.
10. Amer EH. Theoretical and experimental assessment of a double exposure solar cooker. Energy Convers Manag. 2003;44:2651–63.
11. Reddy AR, Narasimha Rao AV. Prediction and experimental verification of performance of box type solar cooker – Part I. Cooking vessel with central cylindrical cavity. Energy Convers Manag. 2007;48:2034–43.
12. Kurt H, Atik K, Ozkaymak M, Recebli Z. Thermal performance parameters estimation of hot box type solar cooker by using artificial neural network. Int J Thermal Sci. 2008;47:192–200.
13. Punia RC, Marwal VK, Sengar N, Dashora P. Numerical modeling of a box-type solar cooker. Int J Thermal Sci. 2012;4:75–83.
14. Verdugo AS. Experimental analysis and simulation of the performance of a box-type solar cooker. Energy Sustain Dev. 2015;29:65–71.
15. Rigollier CH, Bauer O, Wald L. On the clear sky model of the ESRA—European Solar Radiation Atlas—with respect to the Heliosat method. Sol Energy. 2000;68(1):33–48.
16. Hofierka J, Súri M. The solar radiation model for Open source GIS: implementation and applications. In: Proceedings of the Open source GIS—GRASS users conference—Trento, Italy; September 2012. p. 11–13.
17. Kreider JF, Kreith F. Solar energy handbook. McGraw-Hill Book Company; 1981. p. 1099
18. Duffie JA, Beckman WA. Solar engineering of thermal processes. New York: Wiley; 2013.
19. Document, BIS. Indian standards IS 13429: solar cooker - box type, first revision. Manak Bhawan, New Delhi: Bureau of Indian Standards (BIS); 2000.
20. Amante C, Eakins BW. ETOPO1 1 Arc-Minute Global Relief Model: Procedures, Data Sources and Analysis. NOAA Technical Memorandum NESDIS NGDC-24. National Geophysical Data Center, NOAA, 2009.
21. Gschwind B, Mnard L, Albuisson M, Wald L. Three years of experience with the SoDa web service delivering solar radiation information: lessons learned and perspectives. In: Hrebicek J, Racek J, editors. Proceedings of the 19th international conference informatics for environmental protection, part 1. Czech Republic: Published by the Masaryk University in Brno; 2005. p. 95–102.